Electronic Supplementary Material (ESI) for Journal of Materials Chemistry A.
This journal is © The Royal Society of Chemistry 2022

## Supporting Information

# Dual-metal Ni and Fe phthalocyanines/boron-doped g-$C_3N_4$ Z-scheme 2D-heterojuntions for visible-light selective aerobic alcohol oxidation

Haiyue Liu,‡[a] Xiaoyu Chu,‡[bc] Linlu Bai,*[a] Zhaodi Yang,[b] Yuming Jiao,[a] Wensen Li,[b] Yanhong Zhang*[a] and Liqiang Jing*[ab]

[a] Key Laboratory of Functional Inorganic Materials Chemistry (Ministry of Education), School of Chemistry and Materials Science, International Joint Research Center for Catalytic Technology, Heilongjiang University, Harbin 150080, P. R. China.

[b] School of Material Science and Chemical Engineering, Harbin University of Science and Technology, Harbin 150040, P. R. China.

[c] College of Food Engineering, East University of Heilongjiang, Harbin 150066, P. R. China.

## 1. Experimental details

### 1.1 Computational method and details

All geometries were optimized level of the B3LYP hybrid functional in the gas phase.[1] The Stuttgart/Dresden ECP basis sets (SDD) was employed for the Fe and Ni, while the def 2-SVP basis set was used for the other main-group elements. D3 dispersion correction developed by Grimme is included for weak interactions. The stationary frequency calculations at 298.15K and 1 atm were performed at the same level for each of the optimized structures to examine any imaginary frequency or the corresponding vibrational modes. All of these calculations were performed by the Gaussian 16 program package. [2] TDDFT (time-dependent density functional theory) was employed to predict excited state energies and properties to obtain the information of charge transfer. [3]

For giving more reliable interaction energies (Adsorption Energies, $E_{ad}$, or Bonding energies, $E_b$), the Basis Set Superposition Error (BSSE) corrections are carried out. $E_{ad}$ or $E_b$ can be obtained according to the formula $E_{ad}/E_b$ = E_corrected-(E(1) + E(2) +...E(j)... +E(n) ), in which E_corrected = E_complex + E_BSSE and E(j) means the energy doing monomer centered basis set (MCBS) calculation for fragment j.

### 1.2 Hydroxyl radical measurement

Coumarin was used as the labeled molecule to detect the content of the produced hydroxyl radicals. The specific method for the hydroxyl radical test was as follows: 0.02 g of the catalyst was dispersed in 50 mL of coumarin solution at a concentration of $1\times10^{-3}$ M. The mixture was stirred for 30 min before the experiment, to ensure that it reached the adsorption-desorption equilibrium. After light irradiation for 1 h, appropriate amount of the suspension was centrifuged in a 10 mL centrifuge tube and the supernatant was transferred into a Pyrex glass cell for the fluorescence measurement of 7-hydroxycoumarin by a spectrofluorometer (Perkin-Elmer LS55).

### 1.3 Photoelectrochemical and electrochemical measurements

A typical three-electrode system was used to measure photoelec-trochemical (PEC) behavior. The prepared catalyst was used as work in gelectrode, a platinum plate (99.9 %) was served as the counter electrode, a saturated KCl Ag/AgCl electrode was selected to use as there ference electrode, and 0.2 M $Na_2SO_4$ solution as the electrolyte. High purity oxygen gas was bubbled through the electrolyte before and during the experiment. The test was taken in a quartz cell using a 500 W xenon lamp with a cut-off filter ($\lambda > 420$ nm) as the illumination source. The samples were tested the photoelectron chemical performance by an IVIUM V13806 electrochemical workstation. The temperature of each experiment was kept at room temperature (about 25 ºC). Electrochemical (EC) measurements were carried out in the $O_2$-bubbled systems on the same conditions stated above.

### 1.4 $O_2$-temperature programmed desorption

The $O_2$-temperature programmed desorption ($O_2$-TPD) was measured with a home-built flow apparatus. The typical method is as follows: the sample (50 mg) was pre-heated to 200 ºC maintaining for 0.5 h to remove any moisture and then cooled to room temperature under an ultra-high-pure He stream with a flow rate of 30 mL $min^{-1}$. After that, the system was cooled to room temperature and then the sample was blown continuously with $O_2$ for 60 min at 30 ºC. The excess weakly adsorbed $O_2$ was removed by exposure to ultra-high pure He. Then the temperature was increased to 500 ºC with a heating rate of 10 ºC $min^{-1}$ under pure He.

### 1.5 Electron paramagnetic resonance measurements

The $^{\bullet}O_2^-$ radicals usually can be trapped by 5,5-dimethyl-l-pyrroline N-oxide (DMPO), producing the EPR signals of their adducts. The sample (5 mg) was dissolved in DMPO solution with $CH_3OH$ as solvent to obtain the liquid mixture. After illumination, the mixture was characterized using a Bruker EMX plus model spectrometer operating at room temperature.

### 1.6 Photocatalytic performance measurements

Photocatalytic alcohol oxidation: the photocatalyst (20 mg) and the benzyl alcohol as reactant (200 μmol) were added to acetonitrile as solvent (5 mL) within a single flask (30 mL), which was sealed with rubber septum caps, and $O_2$ was bubbled through the solution for 20 min. The flask with the reflux of cooling water was immersed in a temperature-controlled water bath (30 ± 2 ºC) under stirring (600 rpm) and irradiated under visible light using a 300 W Xe lamp ($\lambda > 420$ nm). Dodecane was applied as the external standard. The liquid mixture was analyzed using an Ceaulight gas chromatograph 7920 equipped with a HP-5 capillary column (30 m long and 0.32 mm in diameter, packed with silica-based supelcosil) and flame ionization detector (FID). The injector temperature was 250 ºC and the spilt is 0.05 μL. The column head pressure of the carrier gas nitrogen during the analysis was maintained at 22.57 psi. Temperature program: 120 ºC to 200 ºC; 20 ºC $min^{-1}$; hold for 10 min. The by-products were identified by a gas chromatography-mass spectrometry (GC-MS, Agilent, GC 6890N, MS 5973 inert). The conversion of BA and selectivity of BA/BAD were defined as conversion = $[(C_0 - C_{BA})/C_0] \times 100\%$ and selectivity = $[C_{BAD}/(C_0 - CBA)] \times 100\%$, where $C_0$ is the initial concentration of BA, and $C_{BA}$ and $C_{BAD}$ are the concentrations of the detected BA and BAD, respectively.

Cycling test: after each run for 6 h, the used photocatalyst was separated, washed with deionized water and acetone then dried at 80 °C in the vacuum oven for the next cycle.

## 2. Supplementary Figures and Tables

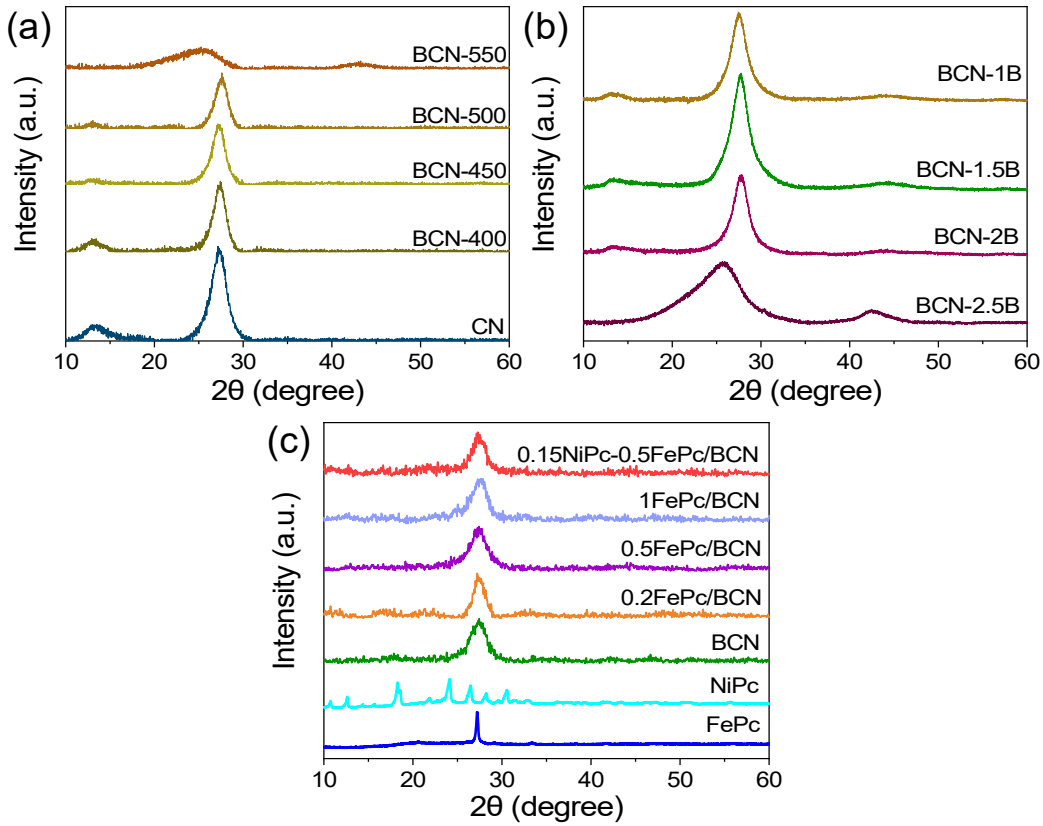


**Figure S1** XRD spectra of (a) CN, BCN-X and (b) BCN-Y, (c) FePc, NiPc, BCN, xFePc/BCN and 0.15NiPc-0.5FePc/BCN, respectively.

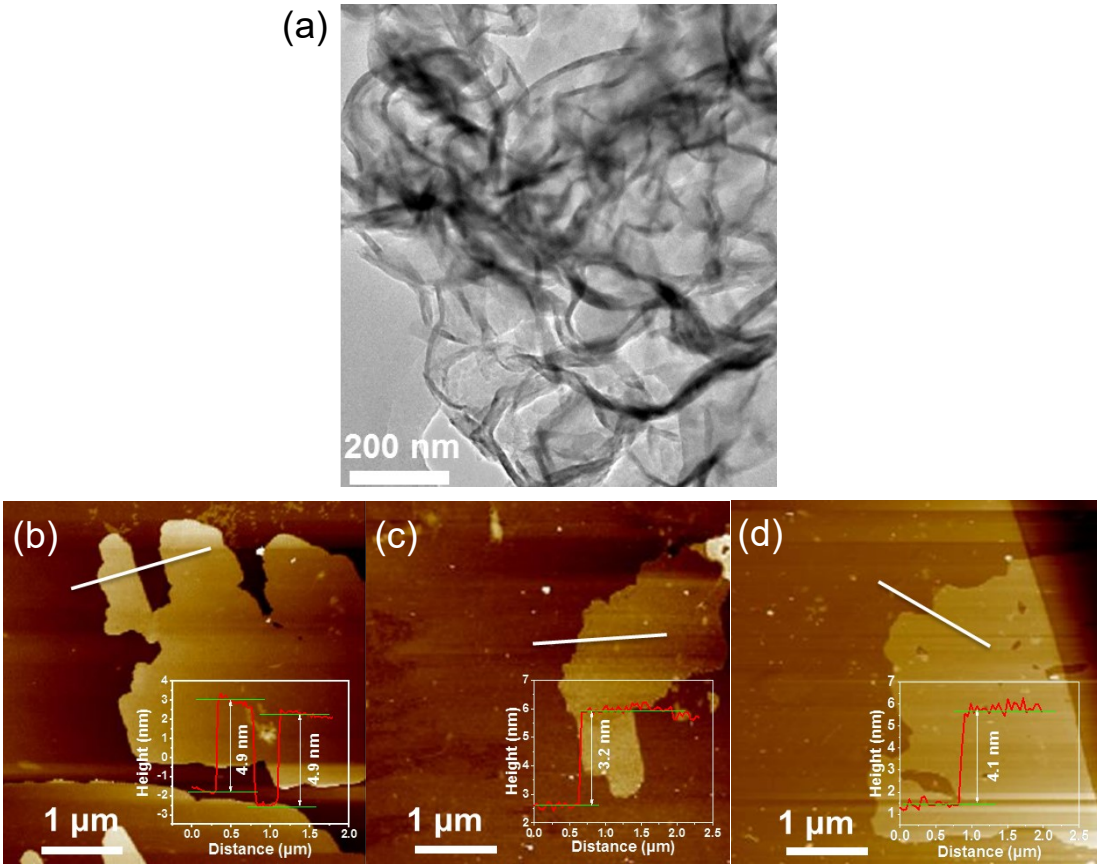


**Figure S2** (a) TEM images of CN, the AFM images and the corresponding height profiles of (b) CN, (c) BCN, and (d) 0.5FePc/BCN, respectively.

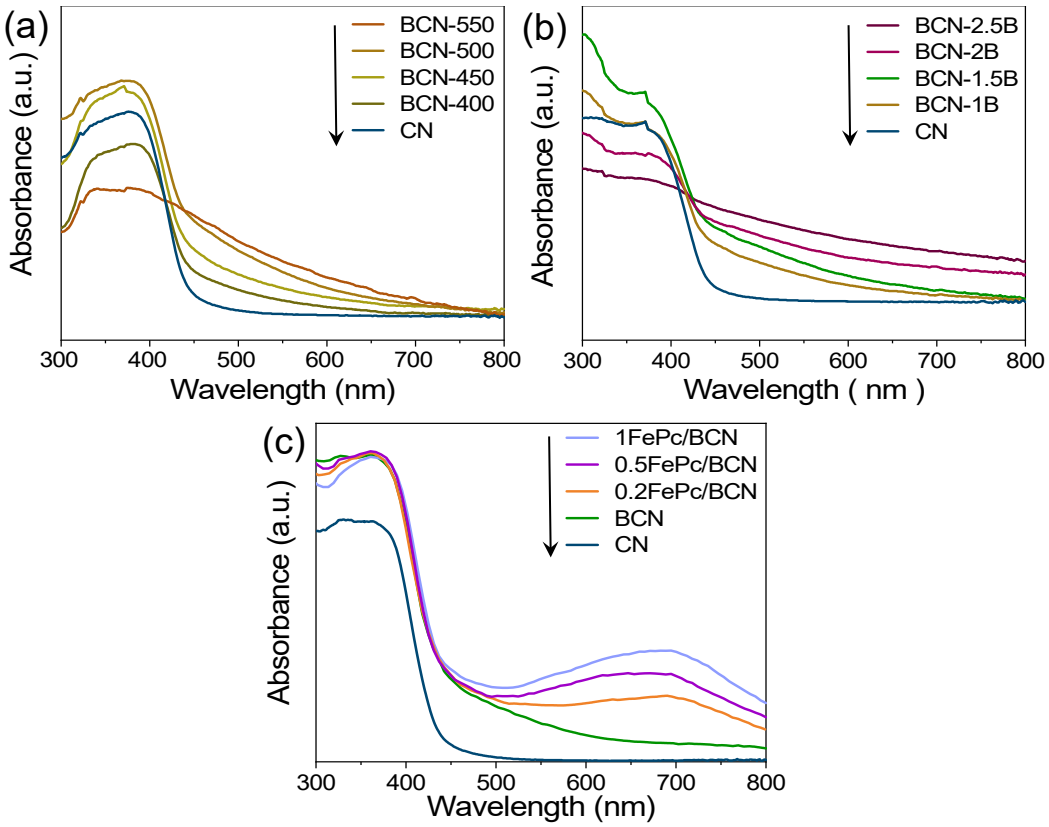


**Figure S3** UV-Vis absorption spectra of (a) CN, BCN-X and (b) CN and BCN-Y. (c) CN, BCN and xFePc/BCN, respectively.

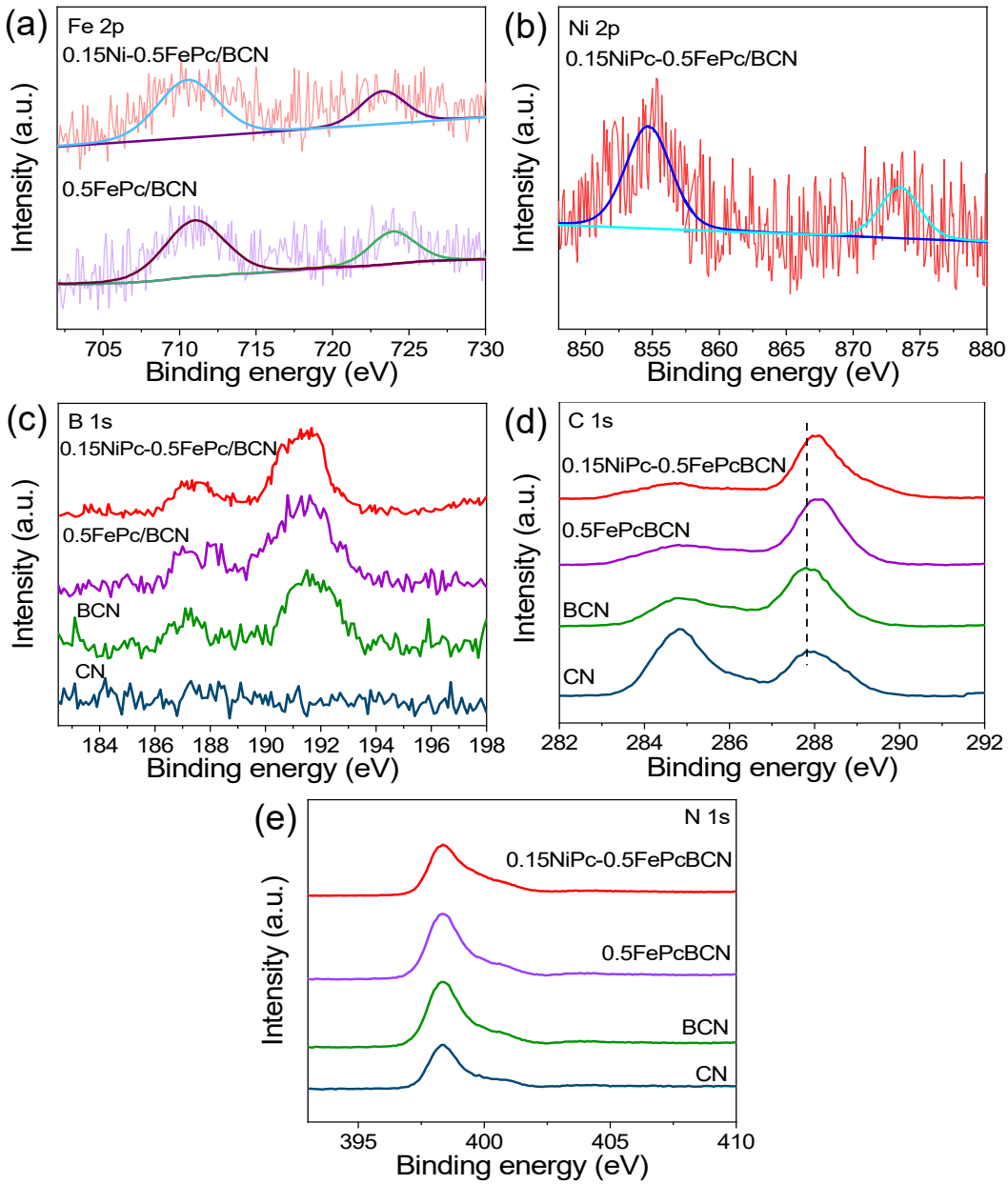


**Figure S4** (a) XPS Fe 2p spectra of 0.5FePc/BCN and 0.15NiPc-0.5FePc/BCN, (b) XPS Ni 2p spectra of 0.15NiPc-0.5FePc/BCN, (c) XPS B 1s spectra of CN, BCN, 0.5FePc/BCN and 0.15NiPc-0.5FePc/BCN, (d) C 1s spectra of CN, BCN, 0.5FePc/BCN and 0.15NiPc-0.5FePc/BCN, (e) N 1s spectra of CN, BCN, 0.5FePc/BCN and 0.15NiPc-0.5FePc/BCN.

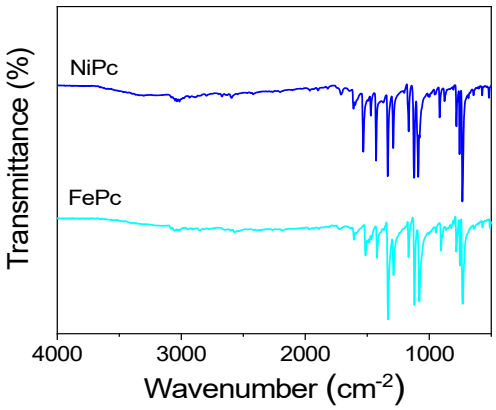


**Figure S5** Normalized fourier transform infrared spectroscopy (FT-IR) of FePc and NiPc, respectively.

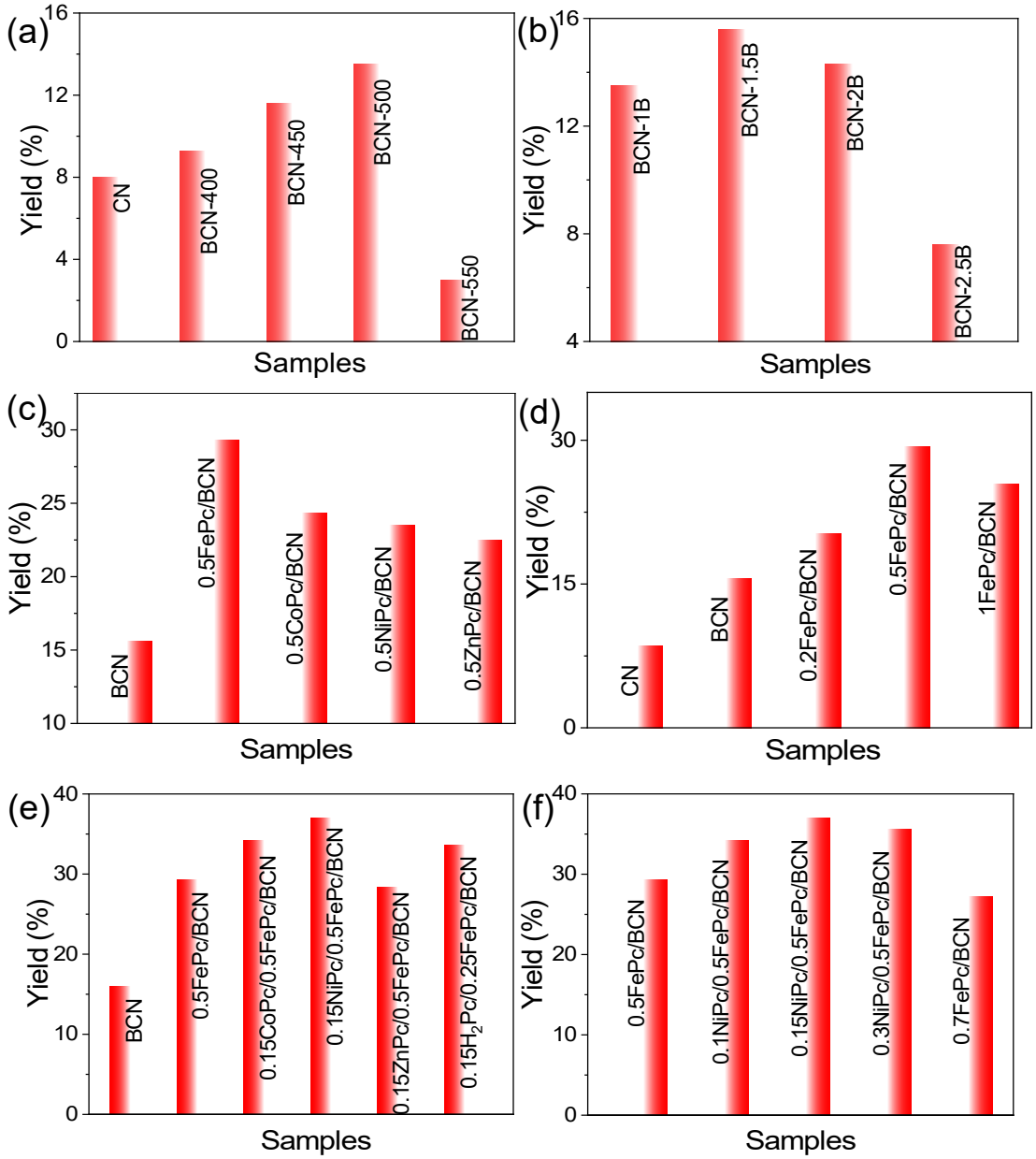


**Figure S6** Photocatalytic activities for benzyl alcohol yield of (a) CN and BCN-X, (b) BCN-Y, (c) BCN and 0.5MPc/BCN, (d) CN, BCN and xFePc/BCN (e) BCN, 0.5FePc/BCN and 0.15MPc-0.5FePc/BCN (f) 0.5FePc/BCN, xFePc/BCN and yNiPc-xFePc/BCN under visible-light irradiation.

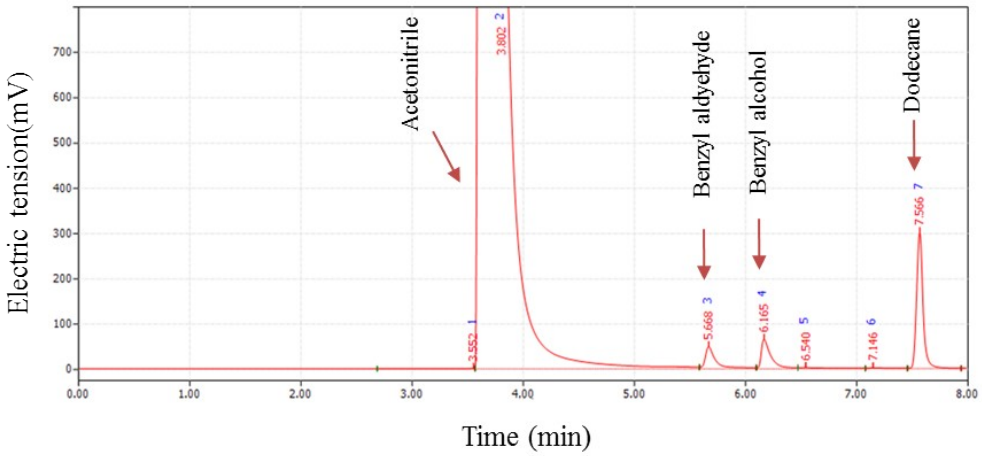


**Figure S7** Corresponding GC peak positions of benzyl alcohol and benzaldehyde.

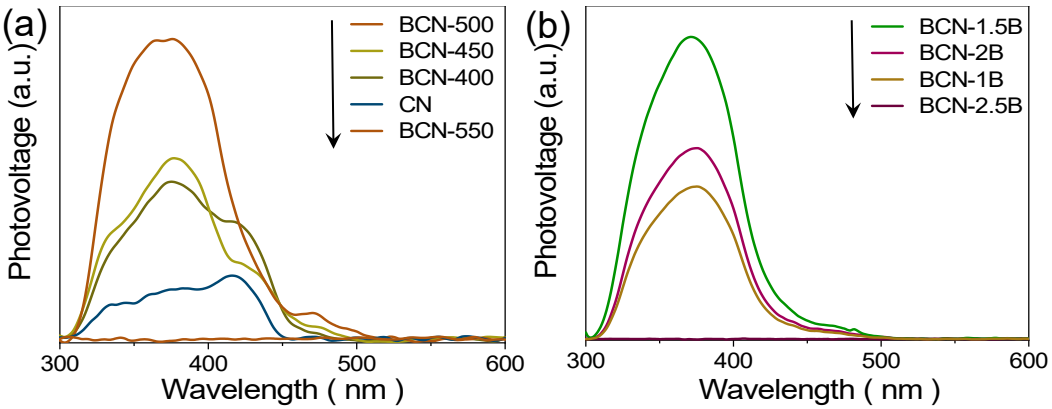


**Figure S8** SPS responses of (a) CN, BCN-X and (b) BCN-Y.

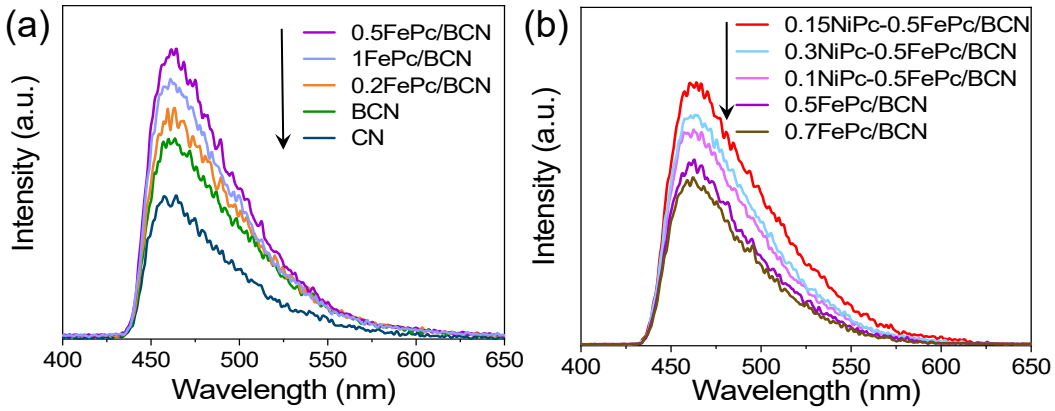


**Figure S9** Fluorescence spectra related to the formed hydroxyl radicals under visible-light irradiation of (a) CN, BCN, xFePc/BCN (b) xFePc/BCN and yNiPc-xFePc/BCN.

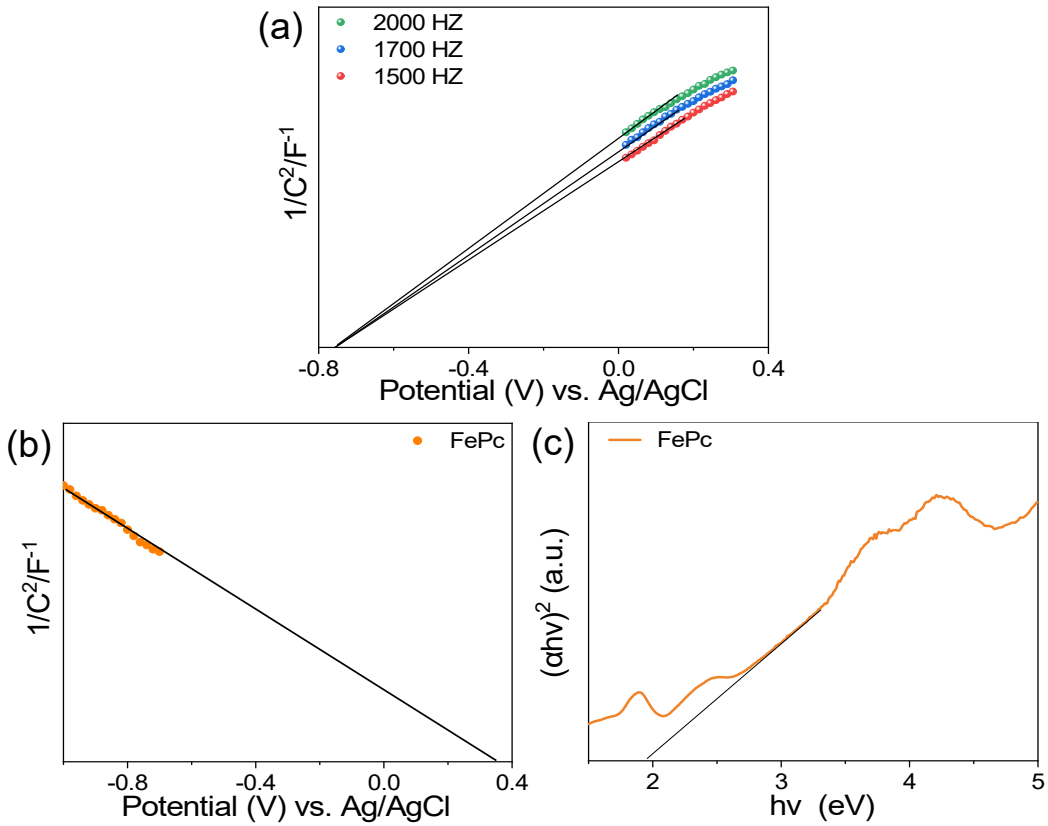


**Figure S10** (a) Mott-Schottky plots for BCN, (b) Mott-Schottky plots for FePc, (c) the plots of transformed Kubelka-Munk function versus photon energy of FePc.

The optical band gap energy ($E_g$) of a semiconductor material could be evaluated by the following formula [4]:

$$\alpha hv = A(hv\text{-}Eg)^{n/2}$$

where α, h, ν, A, and $E_g$ represent the absorption coefficient, planck constant, light frequency, proportionality and band gap energy, respectively. As shown in the Figure. S10c and Figure. S13b, the $E_g$ values for FePc, NiPc are calculated to be 1.99, and 1.95 eV, respectively.

The Mott-Schottky curves for FePc and NiPc were analyzed by the impedance-potential measurements,[5, 6] as shown in Figure. S10b and Figure. S13a, which were determined to be approximately +0.56, +0.58 V for the HOMO levels of FePc, NiPc, respectively. By the following empirical equations [7,8]

$$E_{VB}=E_{CB}+E_{g,}$$

The LUMO levels of FePc, NiPc are calculated to be −1.43 and −1.37 V, respectively.

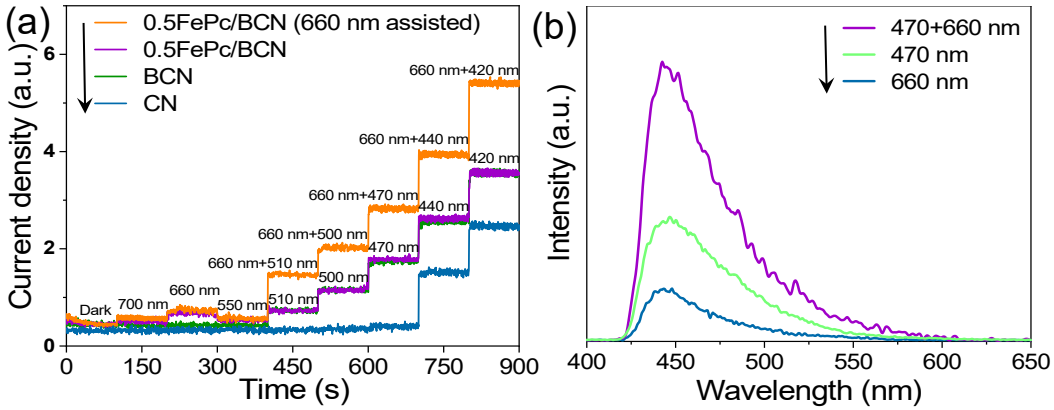


**Figure S11** (a) The monochromatic photocurrent action spectra of CN, BCN, 0.5FePc/BCN, and 0.5FePc/BCN with 660 nm assisted light under different monochromatic light irradiation. (b) Normalized fluorescence spectra related to the formed hydroxyl radicals under 660 nm, 470 nm and double excitation of 0.5FePc/BCN.

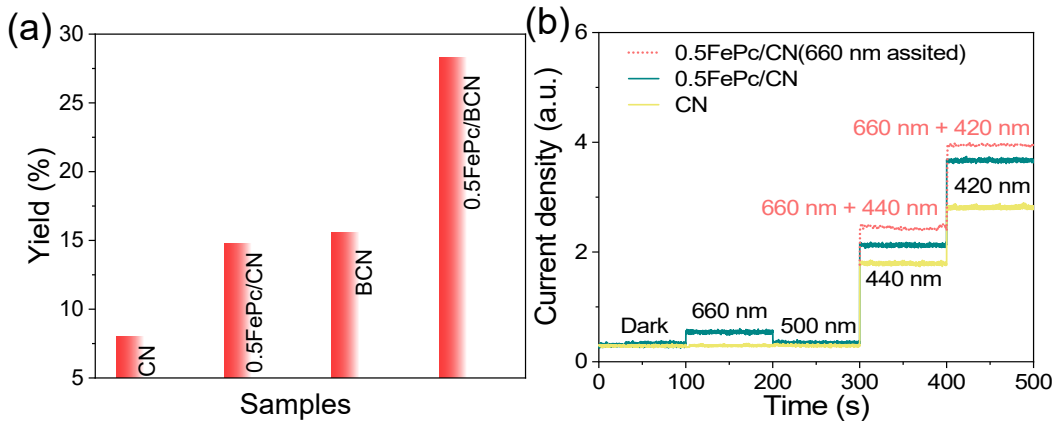


**Figure S12** (a) Photocatalytic activities for benzyl alcohol yield of CN, 0.5FePc/CN, BCN and 0.5FePc/BCN under visible-light irradiation. (b) The monochromatic photocurrent action spectra under different monochromatic light irradiation of CN, 0.5FePc/CN and 0.5FePc/CN with 660 nm assisted light.

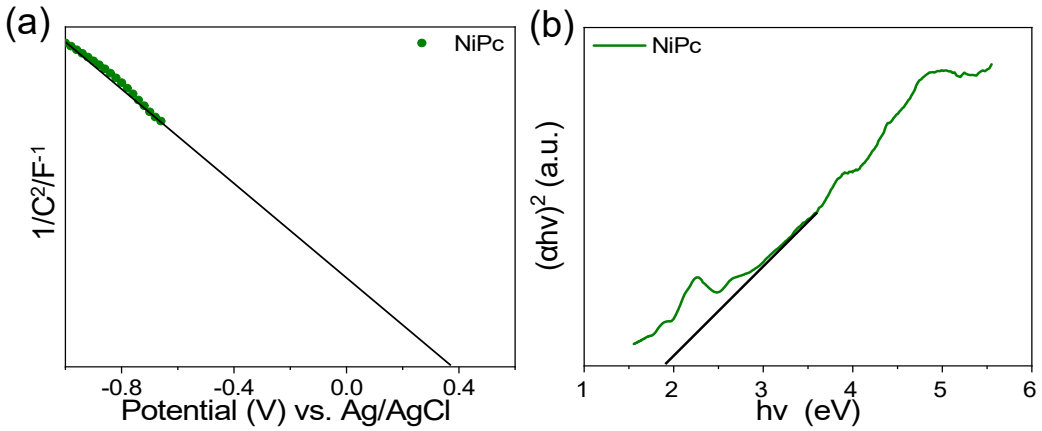


**Figure S13** (a) Mott-Schottky plots for NiPc. (b) The plots of transformed Kubelka-Munk function versus photon energy of NiPc.

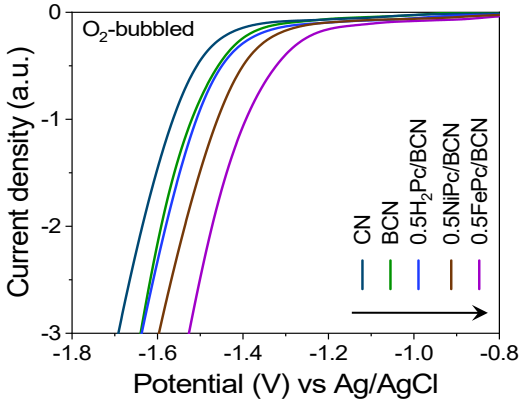


**Figure S14** Electrochemical reduction curves with $O_2$-bubbled of CN, BCN, 0.5$H_2$Pc/BCN, 0.5NiPc/BCN and 0.5FePc/BCN.

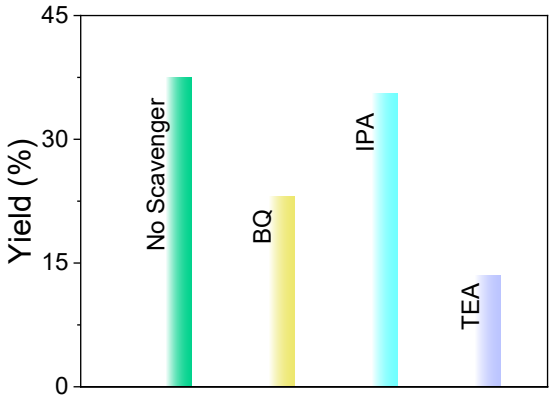


**Figure S15** Photocatalytic activities for benzyl alcohol conversion of 0.15NiPc-0.5FePc/BCN in the presence of the different scavengers.

The active species trapping experiment: tiny amount of scavenger including triethanolamine (TEA), 1,4-benzoquinone (BQ), isopropyl alcohol (IPA) was added in the photocatalytic system, respectively, to find out the effects of the corresponding active species on the photocatalytic reaction. Additionally, TEA (for organic system) are applied as $h^+$ scavenger, BQ as $^{\bullet}O_2^-$ radical scavenger and IPA as $^{\bullet}OH$ radical scavenger, respectively.

**Table S1** Photocatalytic activities of 0.15NiPc-0.5FePc/BCN for selective oxidation of various alcohols.

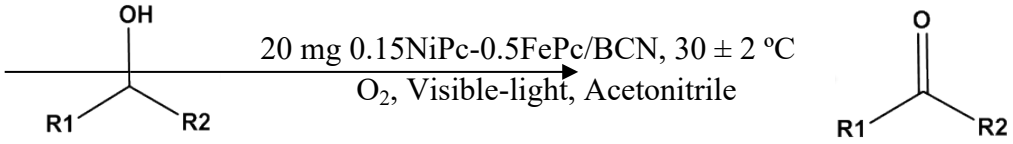


| R1 | R2 | Time (h) | hv | Yield |
|---|---|---|---|---|
| Phenyl | H | 6 | + | 38.5 |
| Phenyl | H | 6 | – | < 3 |
| 4-Methoxyphenyl | H | 6 | + | 46.3 |
| 4-Methylphenyl | H | 6 | + | 43.2 |
| 4-Chlorophenyl | H | 6 | + | 32.1 |
| 4-Nitrophenyl | H | 6 | + | 26.6 |
| $PhCH_2$ | H | 6 | + | 15.3 |
| Phenyl | $CH_3$ | 6 | + | 27.1 |
| 4-Fluorophenyl | H | 6 | + | 29.4 |

**Table S2** Summary of the photocatalytic selective oxidation of BA performance of g-$C_3N_4$ based catalysts.

| Entry | Photocatalyst | Conv. (%) | Select. (%) | Reaction conditions | BAD yield (μmol $g^{-1}$ $h^{-1}$) | Ref. |
|---|---|---|---|---|---|---|
| 1 | 0.15NiPc-0.5FePc/BCN | - | > 99 | Acetonitrile, $O_2$ (1 atm), 300W Xe lamp, (λ > 420 nm), 6 h | 642 | This work |
| 2 | $C_3N_4$-TE-3 | 14 | 77 | $H_2O$, Air, 100 W halogen lamp, (450–750 nm), 4 h | 269.5 | [9] |
| 3 | CMCN | - | - | $H_2O$, 300 W Xe lamp, (420 nm ≤ λ ≤ 780 nm), 20 h | 230 | [10] |
| 4 | $W_{SA}$-CN-PUNS | - | 93.6 | $H_2O$, 300W Xe lamp, (λ > 420 nm), 12 h | 305.1 | [11] |
| 5 | CCN | 52.2 | 92.6 | tri-Fluorotoluene, $O_2$ (1 bar), 300 W Xe lamp, (λ > 420 nm), 60 ºC, 4 h | 151.2 | [12] |
| 6 | mpg-$C_3N_4$/NHPI | 44 | 98 | Acetonitrile, $O_2$ (1atm), 250 W-bulb, (λ > 420 nm), 28 h | 15.4 | [13] |

**References:**

[1] C. Lee, W. Yang, R. G. Parr, *Physical review B.*, 1988, **37**, 785.

[2] M. Frisch, G. Trucks, H. B. Schlegel, G. Scuseria, M. Robb, J. Cheeseman, G. Scalmani, V. Barone, B. Mennucci, G. Petersson, Inc. Wallingford, CT 2009, **200**, 28.

[3] J. D. Chai, M. Head-Gordon, *Phys. Chem. Chem. Phys.*, 2008, **10**, 6615−6620.

[4] T. Y. Shi, H. N. Li, L. J. Ding, F. H. You, L. Ge, Q. Liu, K. Wang, *ACS Sustainable Chem. Eng*. 2019, **7**

3319−3328.

[5] S. P. Adhikari, Z. D. Hood, H. Wang, R. Peng, A. Krall, H. Li, V. W. Chen, K. L. More, Z. L. Wu, S. Geyer, A. Lachgar, *Appl. Catal. B-Environ*., 2017, **217**, 448−458.

[6] L. J. Ye, D. Wang, S. J. Chen, *ACS Appl. Mater. Interfaces*, 2016, **8**, 5280−5289.

[7] F. Chen, Q. Yang, Q. Wang, F. B. Yao, J. Sun, Y. L. Wang, C. Zhang, X. M. Li, C. G. Niu, *Appl. Catal. B-Environ.*, 2017, **209**, 493−505.

[8] Y. Z. Hong, Y. H. Jiang, C. S. Li, W. Q. Fan, X. Yan, M. Yan, W. D. Shi, *Appl. Catal. B-Environ*., 2016, **180**, 663−673.

[9] M. Bellardita, E. I. García-López, G. Marcì, I. Krivtsov, J. R. García, L. Palmisano, *Appl.Catal. B-Environ.*, 2018, **220**, 222−233.

[10] H. F. Wang, J. H. Zhang, X. Jin, X. Q. Wang, F. Zhang, J. R. Xue, Y. P. Li, J. M. Li, *J. Mater. Chem. A* 2021, **9**, 7143−7149.

[11] F. Zhang, J. H. Zhang, H. F. Wang, J. M. Li, H. H. Liu, X. Jin, X. Q. Wang, G. Q. Zhang, *Chem. Eng. Jour.* 2021, **424**, 130004.

[12] M. Zhou, P. J. Yang, R. S. Yuan, A. M. Asiri, M. Wakeel, X. C. Wang, *ChemSusChem*. 2017, **10**, 4451−4456.

[13] P. F. Zhang, J. Deng, J. Y. Mao, H. R. Li, Y. Wang, *Chinese J. Catal.* 2015, **36**, 1580−1586.